Structure of Filter Cakes during the Electroassisted Filtration of Microfibrillated Cellulose

I&EC research
Industrial & Engineering Chemistry Research

pubs.acs.org/IECR

Article

Structure of Filter Cakes during the Electroassisted Filtration of Microfibrillated Cellulose

Anna Lidén, Polina Naidjonoka, Nabin Kumar Karna, and Hans Theliander*

Cite This: https://doi.org/10.1021/acs.iecr.2c03216

Read Online

ACCESS | Metrics & More | Article Recommendations | Supporting Information

ABSTRACT: Microfibrillated cellulose (MFC) is a biobased material with unique properties that can be used in a multitude of applications. Water removal from the dilute product streams is, however, challenging and hinders its commercial attractiveness. One possible method of improving dewatering is the use of electroassisted filtration, in which an electric field is applied across part of the filter chamber. In this work, a bench-scale dead-end filter press, modified to allow for electroassisted filtration, was used to dewater a suspension of MFC produced via 2,2,6,6-tetramethylpiperidinyl-1-oxyl (TEMPO)-mediated oxidation. A filter cake was produced with a channeled structure related to the design of the anode mesh, indicating that the cellulose microfibrils were aligned in the direction of the electric field. This was investigated, qualitatively and quantitively, using scanning electron microscopy and wide-angle X-ray scattering, which showed a preferred orientation on a microscopic level but only a partial orientation on a molecular level (f_c between 0.49 and 0.57). The influence of the density of the anode mesh, in terms of the structure/permeability of the filter cake and dewatering rate, was also evaluated using two different anode mesh densities (5 × 5 and 10 × 10 mm). It was not, however, found to have any major impact on the dewatering rate.

On the structure of filter cakes during the electro-assisted filtration of microfibrillated cellulose

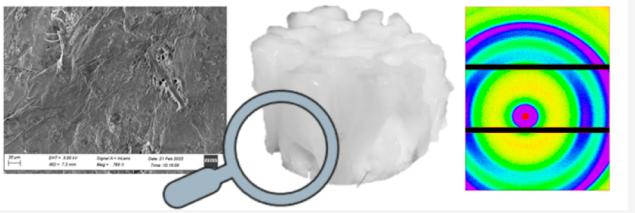

1. INTRODUCTION

Interest in biobased materials has significantly increased in the context of replacing fossil-based resources. Cellulose, the biopolymer most plentiful in nature, makes an excellent candidate. It is found in, e.g., cotton, algae, grass, and trees (40−45% depending on wood species[1]), and its use in various products is already established: from paper products to food and pharmaceuticals. The wide scope of applications based on cellulose is due to its hierarchical structure ranging over multiple length scales with varying functionalities: the fiber structure is typically used in pulp and paper, whereas the polymeric units are used in specialty chemicals, e.g., hydroxymethylcellulose. One current area of interest is the intermediate structures between the fiber and polymeric units, such as microfibrillated cellulose (MFC).

MFC is commonly separated from the cellulose fiber by mechanical means using, e.g., high-pressure homogenizers or grinding; the otherwise high energy demand necessary can be reduced, usually in combination with enzymatical[2] or chemical pretreatment.[3,4] The efforts made to reduce the initial total energy demand since early discoveries were made at the beginning of the 1980s[5,6] have increased the attractiveness of MFC. Particularly successful was the introduction of negative charges on the fibril surface by oxidation of the primary hydroxyls into carboxylate groups through 2,2,6,6-tetramethylpiperidinyl-1-oxyl (TEMPO)-mediated oxidation.[3]

MFCs have crystalline and less crystalline parts, making them flexible and giving them large aspect ratios: they may entangle and form large networks, thereby providing mechanical strength.[7] The surfaces of the cellulose fibrils are covered with a high number of hydroxyl groups, which not only gives the material a high water-holding capacity but also provides excellent opportunities for surface modifications.[8] Applications suggested for MFC include strength agents in paper and board,[9−11] nanocomposites,[12] and oxygen barriers,[13,14] to name but a few.

MFC is processed in dilute streams (typically 2−3%[15]) to avoid too high viscosity and excessive clogging during mechanical separation in high-pressure homogenizers. This, in turn, means that a significant amount of water must be removed in order to reduce costs associated with transport or allow for inclusion in products where water is undesirable. The removal of water from MFC suspensions is, however, challenging because of its characteristics and currently limits its commercial attractiveness.[15,16] Given the excessive amount

Received: September 6, 2022
Revised: September 27, 2022
Accepted: October 6, 2022

of water that needs to be removed, thermal drying techniques are not an option because of the high energy demand. Furthermore, it may also negatively impair the redispersibility of MFC.[17,18] It is therefore important that dewatering techniques requiring less energy are explored.

Among the mechanical dewatering techniques available, filtration is the most common. Filtration of MFC does, however, result in a filter cake with a high filtration resistance, which is mainly due to the low porosity and small particle size and the resulting large surface area that is then subjected to the liquid flow. One way of improving the filtration process is to promote flocculation and thereby reduce the total surface area, e.g., by the addition of ions, as demonstrated by Sim et al.[19] In addition, there are also difficulties in achieving a high final dry content that stem from the great amount of hydroxyl groups present on the surface of MFC, which leads to its high water-holding capacity. A possible alternative for improving the final dry content is therefore to modify the cellulose surface and make it less hydrophilic: Sethi et al.[20] showed that the sonication-assisted modification of cellulose fibrils with hydrophobic lactic acid results in rapid dewatering. Reducing the gel point of the MFC suspension has also been shown to be beneficial.[21−23]

Instead of modifying the MFC suspension, dewatering can be enhanced by using assisted filtration techniques, for example, an electric field (referred to as electroassisted filtration). Applying an electric field across part of the filter chamber introduces various electrokinetic phenomena that affect dewatering and are described in the Theory section. This technique has been used to dewater various kinds of materials that are hard to dewater, e.g., sludges[24−26]

Electroassisted filtration has been used to successfully dewater MFC suspensions and is reported in a patent from 2014,[27] as well as in a recent study based on experimental work and molecular dynamics simulations.[28] The latter employed a filter press with an electric field applied parallel to the flow across the lower part of the filter cell. An interesting observation was made in these particular experiments regarding the structure of the filter cake: the cellulose fibrils were assembled in pillars, and there were channels corresponding to the openings of the anode mesh. The root cause of the filter cake structure was hypothesized to be related to the alignment of cellulose fibrils in the electric field but was not further studied in that specific paper. The orientations of the cellulose fibers and fibrils in an alternating-current electric field have been thoroughly investigated,[29−34] and the indication is that cellulose fibrils tend to align in the direction of the electric field. Studies using a direct-current (dc) electric field are more scarce,[35] and to the authors' knowledge, no studies have been undertaken on the structuring of cellulose particles during electroassisted filtration.

Moreover, because the structure of a filter cake appears to be related to the design of the anode mesh and flow channels are observed in connection to its openings, it would be of importance to examine the design and density of the mesh further because it could affect the overall permeability, and consequently the resistance, of the filter cake.

The present study aims at investigating two observations sprung from the previous study on the electroassisted filtration of MFC[28] that are related to understanding the structure of the filter cake. The first is related to the hypothesis regarding the potential alignment of cellulose fibrils in the electric field and is evaluated both qualitatively and quantitatively using scanning electron microscopy (SEM) and wide-angle X-ray scattering (WAXS), respectively. The second is to evaluate the impact of the design of the anode mesh, with experiments being performed using two anode meshes of different densities.

An improved understanding of the structure of filter cakes will lead to a deeper knowledge of electroassisted filtration. Furthermore, it may also be important to understand how these macroscale structures may be used in, for example, material applications.

2. THEORY

It is well-known that a particle suspended in a polar medium will carry a surface charge due to mechanisms such as ionization and adsorption. According to the electrolytic double layer (EDL) theory, a double layer of counterions will surround the charged particle. The particle's surface charge and EDL will entail electrokinetic properties to the particle when subjected to an electric field.

The major electrokinetic phenomena occurring during the application of a dc electric field are schematically illustrated in Figure 1. The phenomena are depicted for a particle carrying a negative surface charge (like TEMPO-oxidized MFC), and the cathode is placed just beneath a filter medium, whereas the anode is located higher up in the filter chamber. For further details on the electrokinetic phenomena, readers are referred to the review paper by Mahmoud et al.[36]

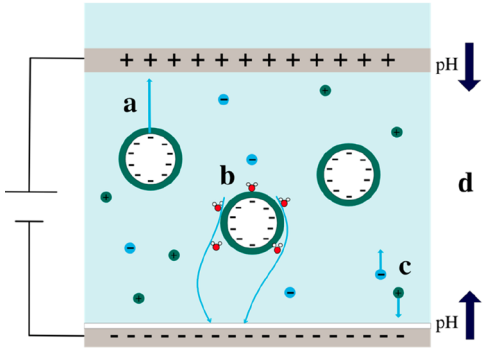

Figure 1. Schematic illustration of the electrokinetic phenomena occurring during electroassisted filtration: electrophoresis (a); electroosmosis (b); ion migration (c); electrolysis reactions (d). Green circles: cations. Blue circles: anions.

Electrophoresis is the movement of suspended charged particles relative to the surrounding liquid (Figure 1a). Particles that carry a negative surface charge will hence migrate toward the anode, which may change the filter cake structure as long as the particle movement is not restricted, e.g., blocked in a filter cake. When this occurs, the effect of electrophoresis becomes negligible and the effect of electro-osmosis starts to dominate.

The electroosmotic flow of water (Figure 1b) is due to migration of the surrounding layer of cations toward the cathode.[37] When this occurs, an adjacent layer of water molecules is transported in the same direction because of viscous drag, and this adds to the volume of filtrate.

Ion migration (Figure 1c) toward each electrode also occurs. Ions may be present in the original suspension or formed in electrolysis reactions (Figure 1d) taking place at that respective electrode:

https://doi.org/10.1021/acs.iecr.2c03216
Ind. Eng. Chem. Res. XXXX, XXX, XXX−XXX

Table 1. Composition (%) of the Dissolving Pulp, including Standard Deviations (n = 5)

glucose	xylose	mannose	ASL[a]	KL[b]	others
91.7 ± 1.3	1.7 ± 0.06	1.0 ± 0.06	0.5 ± 0.03	1.2 ± 0.19	3.9 ± 1.25

[a]ASL = acid-soluble lignin, quantified using UV/vis. [b]KL = Klason lignin, quantified gravimetrically.

$$\text{anode:}\quad 2H_2O(l) \rightarrow 4H^+ + O_2(g) + 4e^-$$
$$M^{n+} + ne^- \rightarrow M$$
$$\text{cathode:}\quad 2H_2O(l) + 2e^- \rightarrow 2OH^- + H_2(g)$$
$$M \rightarrow M^{n+} + ne^-$$

where M is the material of the electrode and M^{n+} its cation.

The formation of hydroxide and hydrogen ions may result in a pH gradient between the electrodes, which may, in turn, have an impact on dewatering if the surface charge of the solid material is sensitive to changes in the pH.[38]

Ohmic heating also occurs as the current passes through the system. This gives rise to a temperature increase that, although it may be beneficial to dewatering due to the viscosity of the liquid decreasing,[39] may also be problematic because an excessively high temperature can harm the filter medium or the solid material.

3. METHODOLOGY

3.1. Materials. MFC was produced from dissolving pulp sourced from a Scandinavian pulp mill. The unoxidized pulp had a carbohydrate composition according to Table 1 and a carboxylate content of 0.025 ± 0.002 mmol/g pulp.[28]

The pulp was subjected to TEMPO-mediated oxidation (see the TEMPO-Mediated Oxidation section) during which the chemicals used were NaClO (10−15% available chlorine) from VWR and TEMPO (98%) and NaBr (>99.5%) from Sigma-Aldrich. NaOH (purity >98%, Sigma-Aldrich) was used to regulate the pH during the oxidation process and absolute ethanol (≥99.8%, VWR) to quench the reaction.

3.2. TEMPO-Mediated Oxidation. The procedure employed is based on work by Brodin and Theliander[40] and explained further by Karna et al.[28] In brief, NaBr (1 mmol/g pulp) and catalytic amounts of TEMPO (0.1 mmol/g pulp) were dissolved in water and added to a pulp suspension in a baffled vessel (⌀ = 0.19 m) under stirring with a four-pitch blade impeller (⌀ = 0.09 m). The reaction was carried out at 1 wt % and at room temperature, being initialized by the dropwise addition of NaClO (5 mmol/g pulp). The pH was maintained at 10 ± 0.05 throughout the reaction by the addition of 0.5 M NaOH; once a reaction time of 70 min had lapsed, the reaction was quenched by the addition of 200 mL of absolute ethanol.

The oxidized fibers were separated from the liquid by vacuum filtration, and in order to retain the smaller fiber fragments, the first two volumes of the filtrate were recycled. The pulp was washed thoroughly with deionized water until the conductivity of the filtrate was stabilized (>23 μS/cm).

3.3. Fibrillated Material. A suspension of 1 wt % MFC, referred to as TEMPO-MFC, was prepared by disintegrating TEMPO-oxidized pulp using IKA Ultra-Turrax T50 with a dispersing element (S50 N-G45F) operating at 10000 rpm. The pulp was treated for 4 min/g and kept in an ice bath during the mechanical treatment to limit the temperature increase. Prior to this treatment, the moisture content of the TEMPO-oxidized pulp was determined by a Sartorius moisture analyzer and performed in a minimum of duplicates.

Characterization of the fibrillated material can be found in the Supporting Information.

3.4. Filtration Equipment. A pneumatically driven, bench-scale filter press[41] modified for electroassisted filtration[42] was used for the experimental work and is depicted schematically in Figure 2. The filter cell has an inner diameter

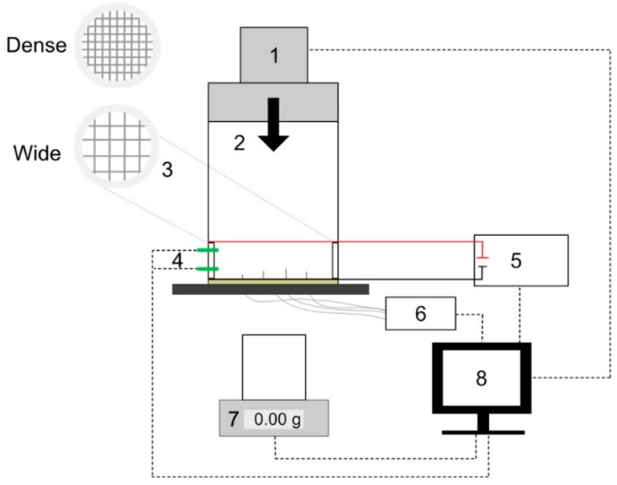

Figure 2. Schematic diagram of the filtration unit: (1) piston press with its position recorded; (2) Plexiglas filter cell, with four pressure capillaries at different heights; (3) close-up of the anode (a mesh of platinum wires with square openings); (4) thermocouples; (5) power supply (current, voltage, and power recorded); (6) pressure transducers; (7) balance; (8) data acquisition unit.

of 60 mm and a total height of 175 mm, of which the lower part (h = 115 mm) is made of plexiglass. A supporting rack of height 30 mm is situated inside the lowest part of the filter cell, thereby reducing the internal diameter to 50 mm. The filter cell is placed on a perforated bottom plate of plastic, upon which a bottom electrode of platinum mesh (Unimesh 300) is positioned. The second electrode, a mesh of platinum wire (⌀ = 0.25 mm) of varying density (see the inset in Figure 2), sets on the supporting rack inside the filter cell. The two electrodes are thus separated at a constant distance of 25 mm and connected to a dc power supply (EA-PSI 5299-02 A, Elektro-Automatik).

The temperature in the filter cell was measured by two PFA-coated K-type thermocouples placed at distances of 5 and 20 mm, respectively, from the filter medium. The temperature, absolute hydrostatic pressure, position of the piston, mass of the filtrate, current, power, and voltage were all logged using *LabVIEW* (software version 15.0, National Instruments), while the mass of the filtrate was weighed using a balance (Mettler Toledo SB 32000).

3.4.1. Experimental Conditions. The filter medium used in all experiments was a hydrophilic poly(ether sulfone) membrane (Supor, PALL) with a nominal pore size of 0.1

https://doi.org/10.1021/acs.iecr.2c03216
Ind. Eng. Chem. Res. XXXX, XXX, XXX−XXX

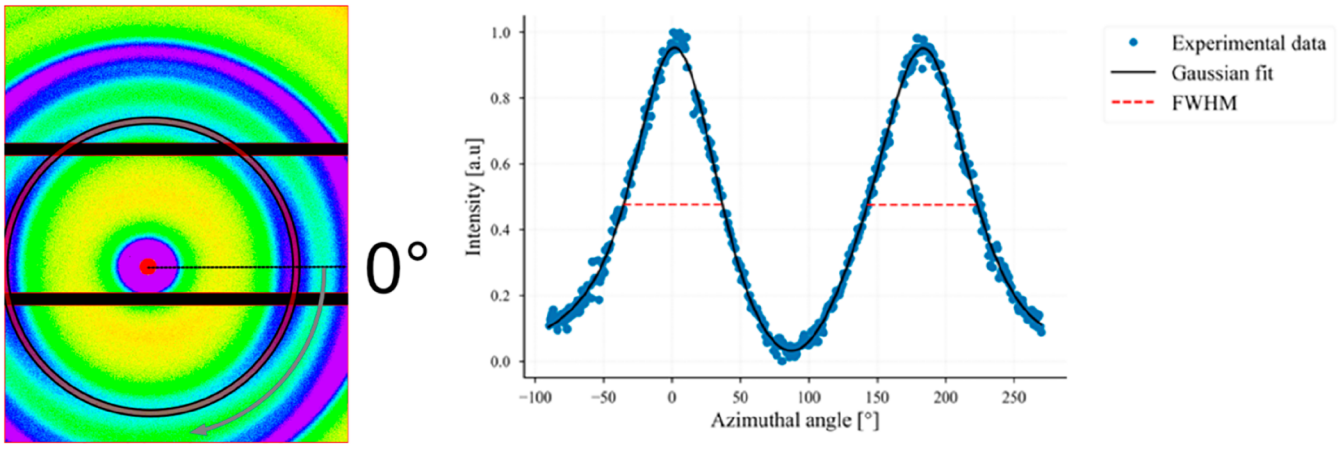

Figure 3. (A) Scattering intensity profile. The red circle illustrates a specific q region and the gray arrow the direction of the azimuthal angle. (B) Azimuthal intensity profile.

μm, along with an underlying support in the form of a Munktell grade 5 filter medium (Ahlström-Munksjö).

A constant applied pressure of 3 bar was used in all electroassisted filtration experiments, and the strength of the electric field applied was either 6 or 24 V/cm. All experiments were run in constant-voltage mode and at room temperature. The mass of the suspension used was weighed prior to each experiment (approximately 500 g). The dewatering rate [g/m^2·s] was calculated by dividing a filtrate mass of 5 g by the time required to obtain the said volume and the filter area.

3.5. Impact of the Mesh Density. The impact of the channeled structure on the dewatering was evaluated by investigating meshes of two different densities: a wide mesh of approximately 10 × 10 mm in size and a dense mesh of approximately 5 × 5 mm in size; see the inset in Figure 2. Two electric field strengths were evaluated: 6 and 24 V/cm.

3.6. Formation of the Channel Structure. The main hypothesis for explaining the channel structure that forms in the filter cake is the alignment of fibrils in the direction of the electric field, so experiments with only an electric field (electroosmotic dewatering) were performed to investigate this. In these, approximately 300 g of a TEMPO-MFC suspension was used, no pressure was applied, and the filter cell was open to the atmosphere.

The alignment of cellulose fibrils in the filter cake formed after electroosmotic dewatering and electroassisted filtration was studied qualitatively and quantitively using SEM and WAXS, respectively. Prior to use, if analyzed in the dry state, the samples taken from the filter cake were dipped in liquid nitrogen and freeze-dried (FreeZone Triad 7400030 freeze-dryer, Labconco Corp.) for 48 h to remove as much water as possible.

3.6.1. SEM. A sharp razor blade was used to obtain thinner sections of the freeze-dried filter cakes; they were then mounted onto a SEM stub with carbon tape. The samples were sputtered with 4 nm of gold using a sputter coater (Leica EM ACE600) before analysis using a LEO Ultra 55 scanning electron microscope operating at an accelerating voltage of 3 kV.

3.6.2. WAXS. Quantitative analysis of the alignment of cellulose fibrils was performed using the Mat:Nordic small-angle X-ray scattering (SAXS)/WAXS/grazing-incidence SAXS, which is equipped with a Cu radiation source (Rigaku 003+ high brilliance microfocus). Following calibration with silver behenate, measurements were run in SAXS and WAXS configurations using a Pilatus 300 K detector and a measurement time between 600 and 900 s. The data treatment was performed using Data Analysis WorkbeNch (DAWN)[43] and ALBULA (Dectris).

Gaussian fitting of the data was performed, whereafter the orientation index (f_c) of the cellulose fibrils in the filter cake was calculated according to eq 1[44−47] from the WAXS data.

$$f_c = \frac{180 - \text{fwhm}}{180} \quad (1)$$

where fwhm corresponds to the full width at half-maximum of the azimuthal intensity distribution profile (Figure 3). A perfectly oriented sample would have a narrow fwhm and a value of f_c approaching 1, whereas a randomly oriented sample would have a value of f_c approaching 0. Although the q region of choice for the azimuthal integration was 1.1 ± 0.05 Å^{-1}, which corresponds to the 1−10/110 plane of cellulose I, the 200 plane can also be used to quantify the orientation because the cellulose crystals are aligned in the direction of the cellulose nanofibrils.

4. RESULTS AND DISCUSSION

4.1. Characterization of TEMPO-MFC. TEMPO-MFC was comprised of both fibrils (width <1 μm) and fibril bundles (width <20 μm), as seen in the SEM micrograph presented in Figure 4.

TEMPO-mediated oxidation successfully introduced carboxylate groups (Figure S1); full details of the ATR-FTIR spectra are given in the Supporting Information. This resulted in a negative ζ potential of −35.1 ± 5.2 mV. A carboxylate content of 1.07 ± 0.02 mmol/g TEMPO-MFC was determined by conductometric titrations; full details on the characterization techniques can be found in the Supporting Information.

4.2. Formation of the Channel Structure. The main hypothesis was that cellulose microfibrils align in the direction of the electric field, and therefore only the use of an electric field, i.e., electroosmotic dewatering, was investigated. It was observed that, after an initial decrease in the current density (Figure S2), the dewatering rate decreased substantially, but in contrast to previous studies, the experiment was continued. It was found, unexpectedly, that dewatering continued, albeit at a significantly lower rate than at the beginning (Figure S3).

https://doi.org/10.1021/acs.iecr.2c03216
Ind. Eng. Chem. Res. XXXX, XXX, XXX−XXX

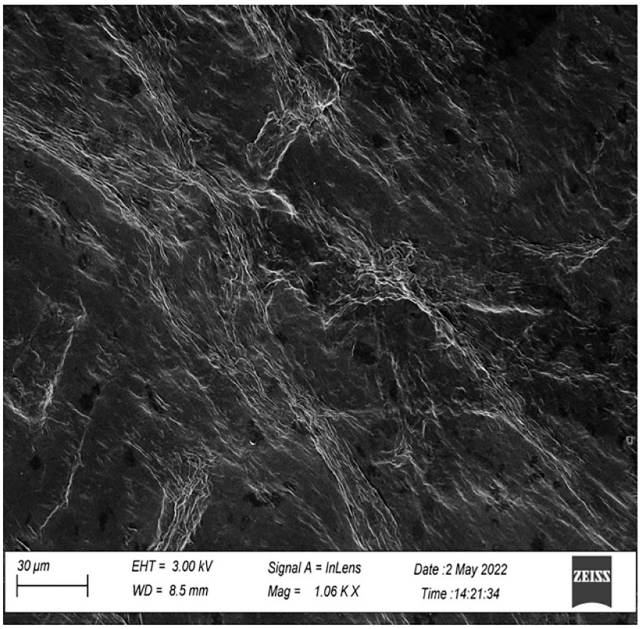

Figure 4. SEM micrograph of TEMPO-MFC.

When the filter cell was opened, the structure shown in Figure 5 was observed: long strands of cellulose fibrils in the direction

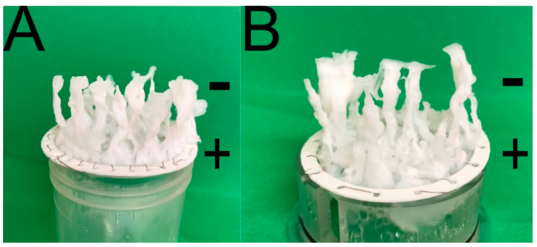

Figure 5. Structures obtained after electroosmotic dewatering at 24 V/cm using denser (a) and wider (b) meshes. Locations of the anode (+) and cathode (−) are as marked.

of the applied electric field. The structure was studied using SEM (Figure 6), which indicated the preferred orientation in the electric field on the microscopic level. Additional SEM micrographs can be found in Figure S4.

The use of electroassisted filtration resulted in denser filter cakes with channels corresponding to the holes of the anode mesh. Images of the filter cakes produced using applied electric field strengths of 6 and 24 V/cm respectively are shown in Figures 7a and 8a. It appears, from visual inspection, that a stronger electric field results in a filter cake with a more pronounced channeled structure.

Observations made after the use of SEM, as shown in Figures 7b−d and 8b−d, revealed intricate structures with varying porosity and orientation, making the recognition of clear trends challenging. There did, nevertheless, appear to be regions with a preferred orientation in both filter cakes, although these were more pronounced when a greater electric field strength was applied. SEM micrographs of higher magnification can be found in Figure S5.

4.2.1. WAXS Measurements. The molecular orientation of cellulose fibrils within the filter cakes was analyzed by WAXS in both the wet and freeze-dried states. The azimuthal curve of fibrils in wet filter cakes showed no clear orientation. The scattering intensity and distribution is dependent on the density of scattering centers or, as in this case, crystallites. The distance between the crystallite centers increases as the fibrils swell, leading to a lower scattering density.[48] The decrease in the degree of orientation that occurs with swelling has been observed previously for cellulose fibers spun from different solutions.[49] The swelling of cellulose fibrils can be observed from the SAXS data (Figure S6), where the scattering curve of fibrils in the wet state shows a broad peak centered at around 0.07 $Å^{-1}$,[50,51] which is characteristic of interfibrillar distances. This peak is absent in the curve of a dry filter cake because the distance is too large to capture with SAXS. Further, the molecular orientation of cellulose fibrils was determined in the dried state.

The risk of introducing a preferential orientation of the cellulose fibrils during water removal was mitigated by employing a method based on flash freezing in liquid nitrogen followed by freeze-drying. This method was shown by Zhang et al.[52] to be the most effective in preserving the highly porous network structure of MFC hydrogels compared to slow freezing (−80 and −20 °C).

The azimuthal profile of the freeze-dried TEMPO-MFC was run as a reference and shows an isotropic pattern (Figure 9), which corresponds to a random orientation. The filter cakes obtained using electroassisted filtration did, however, display anisotropic features, as seen in Figure 10a; this was also true

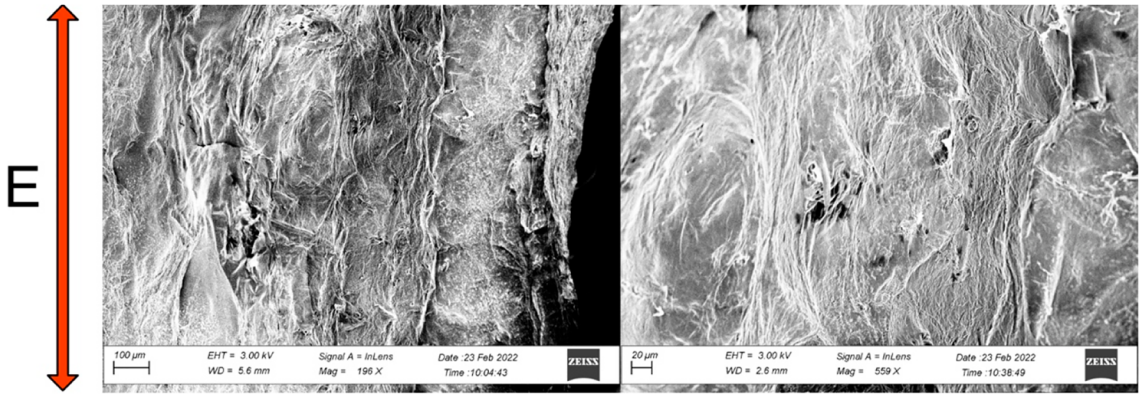

Figure 6. SEM micrographs of structures obtained after electroosmotic dewatering at 24 V/cm (wide mesh). The direction of the electric field, *E*, is vertical.

https://doi.org/10.1021/acs.iecr.2c03216
Ind. Eng. Chem. Res. XXXX, XXX, XXX−XXX

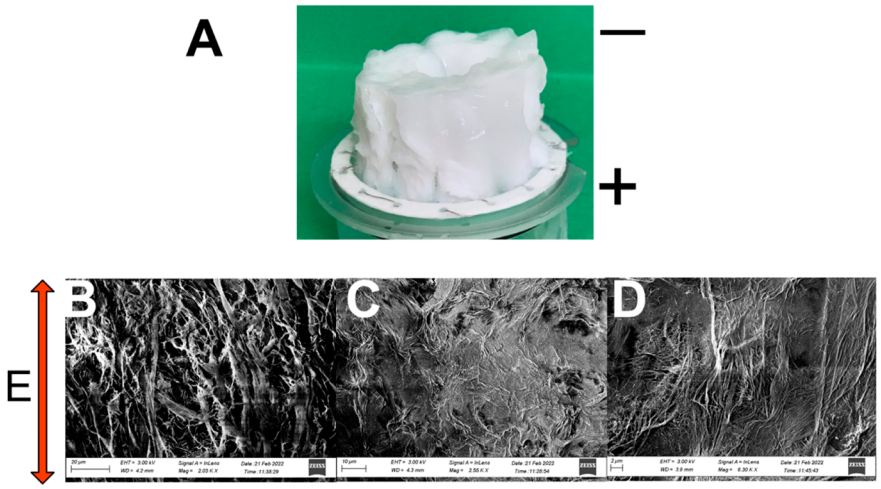

Figure 7. (A) Image of a filter cake after electroassisted filtration using 6 V/cm, showing the locations of the anode (+) and cathode (−). (B−D) SEM micrographs of varying magnification. The direction of the electric field, *E*, is vertical.

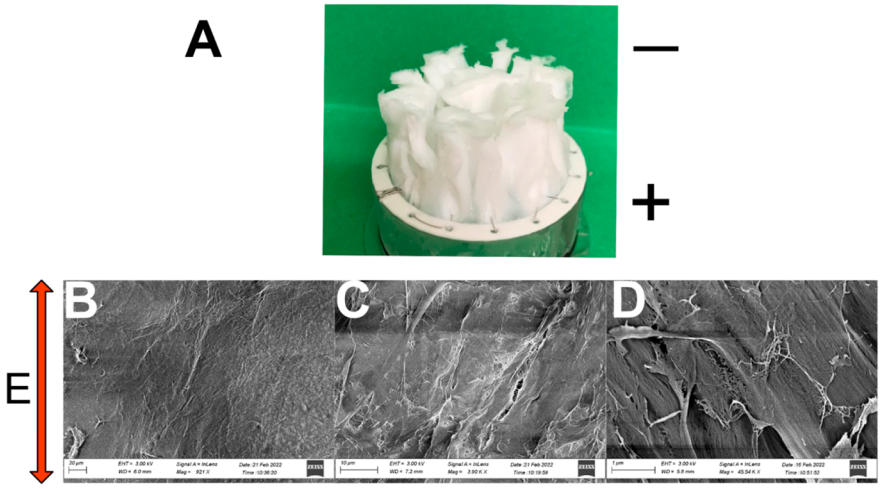

Figure 8. (A) Image of a filter cake after electroassisted filtration using 24 V/cm, showing the locations of the anode (+) and cathode (−). (B−D) SEM micrographs of varying magnification. The direction of the electric field, *E*, is vertical.

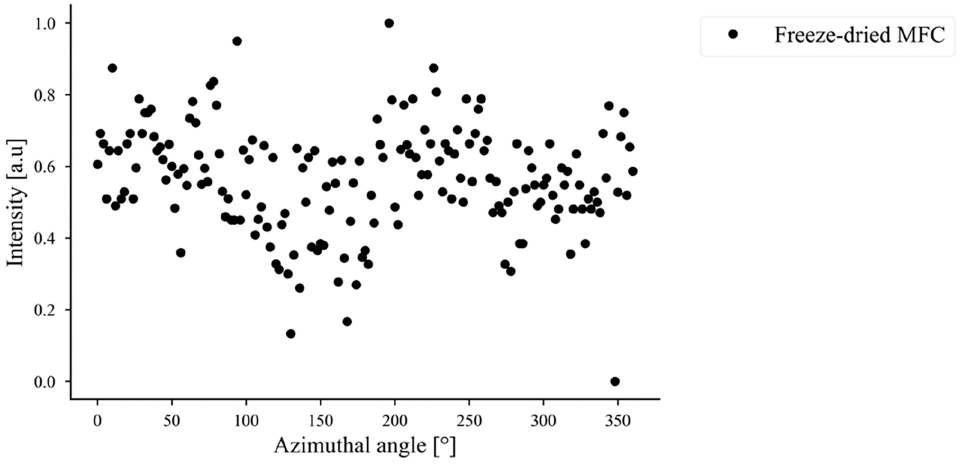

Figure 9. Azimuthal intensity profile of freeze-dried MFC.

for the structures obtained using electroosmotic dewatering. The orientation index, f_o, was calculated from the azimuthal profile according to eq 1. The orientation indexes, including the result for electroosmotic dewatering, are summarized in the bar chart in Figure 10b. The values obtained vary between 0.49 and 0.57, depending on the applied pressure and electric field

https://doi.org/10.1021/acs.iecr.2c03216
Ind. Eng. Chem. Res. XXXX, XXX, XXX−XXX

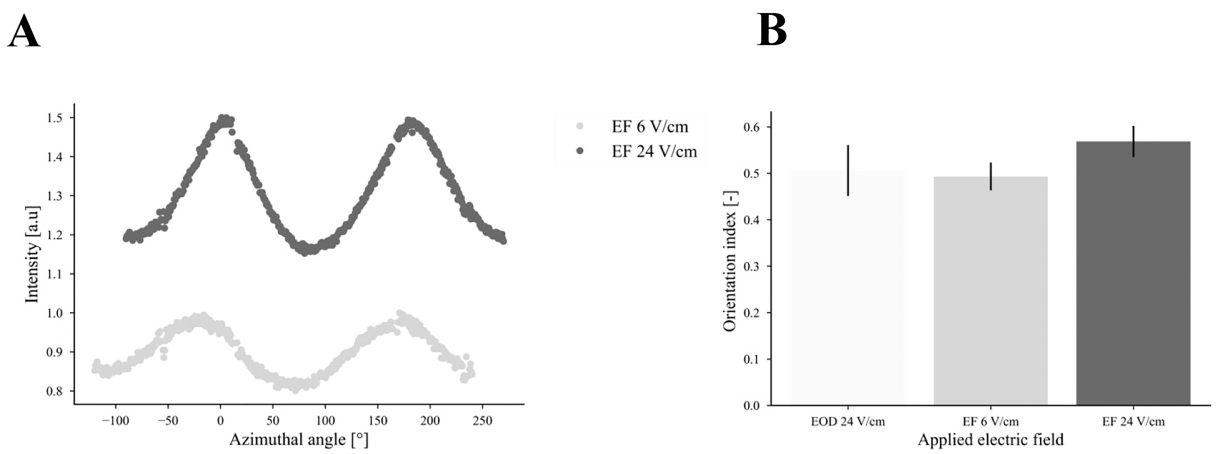

Figure 10. (A) Azimuthal intensity profile. (B) Orientation index, including standard deviation. EOD = electroosmotic dewatering; EF = electroassisted filtration.

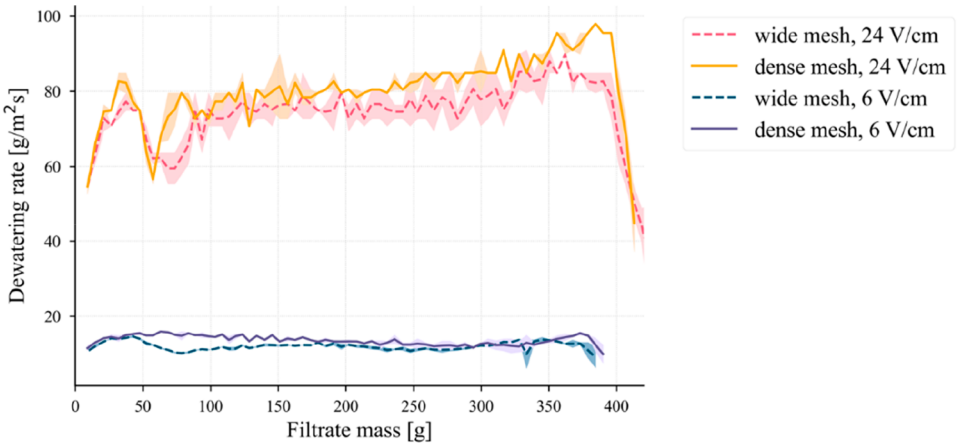

Figure 11. Dewatering rate versus mass of filtrate. Shaded area: standard deviations from duplicate measurements. Dashed and solid lines: experiments using wide and dense meshes, respectively. The applied pressure was kept constant at 3 bar.

strength, which indicates a partial preferred orientation. These values may appear low in comparison with other published studies on the cellulose fibril orientation using WAXS. Mittal et al.,[53] for example, used a flow-focusing system to align dilute suspensions of TEMPO-oxidized cellulose nanofibers (3 g/L) into filaments and reported orientation indexes between 0.83 and 0.92. The impossibility of making comparisons between such studies, because of differences in the experimental setup and sample preparation, should, nonetheless, be emphasized. In the present study, with a much higher concentration of MFC and lower flow rates, the fibrils will not have the possibility to orient fully because of, e.g., entanglements, and it is, thus, expected that the orientation index becomes lower.

The orientation index increases slightly as the electric field strength increases: increasing it from 6 to 24 V/cm caused the orientation index to increase from 0.49 to 0.57. It is important to take into consideration the time that microfibrils have for orientation in the electric field: the experiments at 6 V/cm took 250 min, whereas at 24 V/cm, only 45 min was required. The effect of the electric field is time-dependent because the mobility of the cellulose fibrils becomes restricted as the concentration of the particles increases.

When only an external electric field is applied and no pressure, the resulting orientation index is 0.51, which is slightly lower than that found for electroassisted filtration experiments at the same strength. The somewhat lower orientation could be explained partially by the high electrical resistance (Figure S2; drop in the current density) possibly due to the local formation of gas at the electrodes. Another plausible reason could be that the flow through the filter cell is considerably higher when pressure is applied (cf. Figures 11 and S3) and that this, in turn, could stabilize the structure and straighten out the mechanical interlocking and bent fibrils.

4.3. Impact of the Mesh Density. The impact of the anode mesh density on dewatering was determined by evaluating two different meshes at two levels of applied electric field. The results are shown in Figure 11, which displays the dewatering rate versus filtrate mass during electroassisted filtration. It is obvious that a higher electric field strength results in a remarkably higher dewatering rate: despite the tendency that a dense mesh gives a slightly higher dewatering rate, the effect is, nevertheless, small and more or less within the experimental error. The density of the anode mesh therefore does not appear to have a pronounced impact on the dewatering rate under the circumstances investigated.

One surprising observation is that the dewatering rate reaches an almost constant value: this has not been observed in earlier studies of electroassisted filtration (e.g., refs 26 and 54), where instead the trend has been a declining dewatering rate due to the formation of a filter cake. A reasonable explanation

https://doi.org/10.1021/acs.iecr.2c03216
Ind. Eng. Chem. Res. XXXX, XXX, XXX−XXX

for the approximately constant dewatering rate is that, as a result of the formation of the pillars of TEMPO-MFC, there will be areas on the filter medium that have a very thin filter cake of TEMPO-MFC that does not grow, and this area becomes more or less constant. In addition, this also implies that it is the pillars of cellulose that grow during the filtration.

The density of the mesh has an impact on the uniformity of the electric field: a denser mesh results in a more uniform electric field.[55] This should in theory favor dewatering because the regions with a lower electric field strength would be smaller/fewer and thus the overall electric field strength higher. Moreover, the mesh density also has an impact on the structure of the filter cake produced because flow channels are associated with the openings of the anode mesh and thereby the area of the filter medium exposed. This, in turn, could theoretically affect dewatering: larger flow channels and area of the filter medium exposed (associated with a wider mesh) would be assumed to be favorable, whereas narrower channels (associated with a denser mesh) would not. The trade-off between the density of the electric field and the size of the flow channels did, however, seem to balance each other because no difference could be observed between the two mesh densities.

5. CONCLUSIONS

A channeled filter cake structure was observed when using electroassisted filtration to dewater TEMPO-MFC. The alignment of cellulose fibrils in the filter cakes in the presence of an electric field was evaluated using SEM and WAXS. Visual observations of the filter cake indicate that cellulose microfibrils align in the direction of the electric field, and this was also observed on microscale using SEM. Using WAXS (i.e., on the molecular scale), only a partial preferred orientation was detected, which may be because the cellulose microfibrils are not perfectly aligned but entanglements and bent fibrils may be present.

Two different anode mesh densities were evaluated to determine the impact of the channeled structure on the overall permeability and, hence, the dewatering rate, but no difference was found in terms of the dewatering rate under the conditions investigated.

■ ASSOCIATED CONTENT

Supporting Information

The Supporting Information is available free of charge at https://pubs.acs.org/doi/10.1021/acs.iecr.2c03216.

Details of the characterization techniques used for TEMPO-MFC and additional results of electroosmotic dewatering, SEM micrographs, and SAXS (PDF)

■ AUTHOR INFORMATION

Corresponding Author

Hans Theliander − *Department of Chemistry and Chemical Engineering, Chalmers University of Technology, SE-41296 Gothenburg, Sweden; Wallenberg Wood Science Center, The Royal Institute of Technology, Chalmers University of Technology and Linköping University, SE-10044 Stockholm, Sweden;* orcid.org/0000-0002-2120-6513; Email: hanst@chalmers.se

Authors

Anna Lidén − *Department of Chemistry and Chemical Engineering, Chalmers University of Technology, SE-41296 Gothenburg, Sweden;* orcid.org/0000-0002-0169-1398

Polina Naidjonoka − *Department of Physics, Chalmers University of Technology, SE-41296 Gothenburg, Sweden*

Nabin Kumar Karna − *Department of Chemistry and Chemical Engineering, Chalmers University of Technology, SE-41296 Gothenburg, Sweden; Wallenberg Wood Science Center, The Royal Institute of Technology, Chalmers University of Technology and Linköping University, SE-10044 Stockholm, Sweden;* orcid.org/0000-0002-2496-9647

Complete contact information is available at: https://pubs.acs.org/10.1021/acs.iecr.2c03216

Notes

The authors declare no competing financial interest.

■ ACKNOWLEDGMENTS

This work was performed, in part, at the Chalmers Material Analysis Laboratory. Financial aid received from The Swedish Research Council (Vetenskapsrådet) is gratefully acknowledged as well as from Knut and Alice Wallenberg Foundation, through Wallenberg Wood Science Center (WWSC). Dr. Stefan Gustafsson is thanked for his assistance with SEM analysis. Maureen Sondell is thanked for her assistance with the language review.

■ REFERENCES

(1) Sjöström, E.The Structure of Wood. In *Wood Chemistry*, 2nd ed.; Sjöström, E., Ed.; Academic Press: San Diego, 1993; Chapter 1, pp 1−20. DOI: 10.1016/B978-0-08-092589-9.50005-X.

(2) Pääkkö, M.; Ankerfors, M.; Kosonen, H.; Nykänen, A.; Ahola, S.; Österberg, M.; Ruokolainen, J.; Laine, J.; Larsson, P. T.; Ikkala, O.; Lindström, T. Enzymatic Hydrolysis Combined with Mechanical Shearing and High-Pressure Homogenization for Nanoscale Cellulose Fibrils and Strong Gels. *Biomacromolecules* **2007**, *8* (6), 1934−1941.

(3) Saito, T.; Isogai, A. TEMPO-Mediated Oxidation of Native Cellulose. The Effect of Oxidation Conditions on Chemical and Crystal Structures of the Water-Insoluble Fractions. *Biomacromolecules* **2004**, *5* (5), 1983−1989.

(4) Wågberg, L.; Winter, L.; Ödberg, L.; Lindström, T. On the Charge Stoichiometry upon Adsorption of a Cationic Polyelectrolyte on Cellulosic Materials. *Colloids Surf.* **1987**, *27* (1), 163−173.

(5) Turbak, A. F.; Snyder, F. W.; Sandberg, K. R.Microfibrillated Cellulose, a New Cellulose Product: Properties, Uses, and Commercial Potential. *J. Appl. Polym. Sci.: Appl. Polym. Symp. (United States)***1983**, *37*.

(6) Herrick, F. W.; Casebier, R. L.; Hamilton, J. K.; Sandberg, K. R.Microfibrillated Cellulose: Morphology and Accessibility. *J. Appl. Polym. Sci.: Appl. Polym. Symp. (United States)***1983**, *37*.

(7) Lu, J.; Askeland, P.; Drzal, L. T. Surface Modification of Microfibrillated Cellulose for Epoxy Composite Applications. *Polymer* **2008**, *49* (5), 1285−1296.

(8) Stenstad, P.; Andresen, M.; Tanem, B. S.; Stenius, P. Chemical Surface Modifications of Microfibrillated Cellulose. *Cellulose* **2008**, *15* (1), 35−45.

(9) Winter, A.; Gindl-Altmutter, W.; Mandlez, D.; Bauer, W.; Eckhart, R.; Leitner, J.; Veigel, S. Reinforcement Effect of Pulp Fines and Microfibrillated Cellulose in Highly Densified Binderless Paperboards. *Journal of Cleaner Production* **2021**, *281*, 125258.

(10) Eriksen, O.; Syverud, K.; Gregersen, O. The Use of Microfibrillated Cellulose Produced from Kraft Pulp as Strength Enhancer in TMP Paper. *Nordic Pulp & Paper Res. J.* **2008**, *23* (3), 299−304.

(11) Brodin, F. W.; Gregersen, Ø. W.; Syverud, K. Cellulose Nanofibrils: Challenges and Possibilities as a Paper Additive or Coating Material - A Review. *Nordic Pulp & Paper Research Journal* **2014**, *29* (1), 156−166.
(12) Kumode, M. M. N.; Bolzon, G. I. M.; Magalhães, W. L. E.; Kestur, S. G. Microfibrillated Nanocellulose from Balsa Tree as Potential Reinforcement in the Preparation of 'Green' Composites with Castor Seed Cake. *Journal of Cleaner Production* **2017**, *149*, 1157−1163.
(13) Belbekhouche, S.; Bras, J.; Siqueira, G.; Chappey, C.; Lebrun, L.; Khelifi, B.; Marais, S.; Dufresne, A. Water Sorption Behavior and Gas Barrier Properties of Cellulose Whiskers and Microfibrils Films. *Carbohydr. Polym.* **2011**, *83* (4), 1740−1748.
(14) Lavoine, N.; Desloges, I.; Khelifi, B.; Bras, J. Impact of Different Coating Processes of Microfibrillated Cellulose on the Mechanical and Barrier Properties of Paper. *J. Mater. Sci.* **2014**, *49* (7), 2879−2893.
(15) Sinquefield, S.; Ciesielski, P. N.; Li, K.; Gardner, D. J.; Ozcan, S. Nanocellulose Dewatering and Drying: Current State and Future Perspectives. *ACS Sustainable Chem. Eng.* **2020**, *8* (26), 9601−9615.
(16) Shatkin, J. A.; Wegner, T. H.; Bilek, E. M.; Cowie, J. Market Projections of Cellulose Nanomaterial-Enabled Products - Part 1: Applications. *TAPPI J.* **2014**, *13* (5), 9−16.
(17) Peng, Y.; Gardner, D. J.; Han, Y. Drying Cellulose Nanofibrils: In Search of a Suitable Method. *Cellulose* **2012**, *19* (1), 91−102.
(18) Žepič, V.; Fabjan, E. Š.; Kasunič, M.; Korošec, R. C.; Hančič, A.; Oven, P.; Perše, L. S.; Poljanšek, I. Morphological, Thermal, and Structural Aspects of Dried and Redispersed Nanofibrillated Cellulose (NFC). *Holzforschung* **2014**, *68* (6), 657−667.
(19) Sim, K.; Lee, J.; Lee, H.; Youn, H. J. Flocculation Behavior of Cellulose Nanofibrils under Different Salt Conditions and Its Impact on Network Strength and Dewatering Ability. *Cellulose* **2015**, *22* (6), 3689−3700.
(20) Sethi, J.; Oksman, K.; Illikainen, M.; Sirviö, J. A. Sonication-Assisted Surface Modification Method to Expedite the Water Removal from Cellulose Nanofibers for Use in Nanopapers and Paper Making. *Carbohydr. Polym.* **2018**, *197*, 92−99.
(21) Li, Q.; Raj, P.; Husain, F. A.; Varanasi, S.; Rainey, T.; Garnier, G.; Batchelor, W. Engineering Cellulose Nanofibre Suspensions to Control Filtration Resistance and Sheet Permeability. *Cellulose* **2016**, *23* (1), 391−402.
(22) Varanasi, S.; Batchelor, W. Superior Non-Woven Sheet Forming Characteristics of Low-Density Cationic Polymer-Cellulose Nanofibre Colloids. *Cellulose* **2014**, *21* (5), 3541−3550.
(23) Raj, P.; Varanasi, S.; Batchelor, W.; Garnier, G. Effect of Cationic Polyacrylamide on the Processing and Properties of Nanocellulose Films. *J. Colloid Interface Sci.* **2015**, *447*, 113−119.
(24) Gingerich, I.; Neufeld, R. D.; Thomas, T. A. Electroosmotically Enhanced Sludge Pressure Filtration. *Water Environment Research* **1999**, *71* (3), 267−276.
(25) Conrardy, J.-B.; Vaxelaire, J.; Olivier, J. Electro-Dewatering of Activated Sludge: Electrical Resistance Analysis. *Water Res.* **2016**, *100*, 194−200.
(26) Olivier, J.; Conrardy, J.-B.; Mahmoud, A.; Vaxelaire, J. Electro-Dewatering of Wastewater Sludge: An Investigation of the Relationship between Filtrate Flow Rate and Electric Current. *Water Res.* **2015**, *82*, 66−77.
(27) Heiskanen, I.; Backfolk, K.; Kotilainen, A.; Gaidelis, V.; Sidaravicius, J.Process for Treating Microfibrillated Cellulose and Microfibrillated Cellulose Treated According to the Process. U.S, Patent US20140088301A1, March 27, 2014.
(28) Karna, N. K.; Lidén, A.; Wohlert, J.; Theliander, H. Electroassisted Filtration of Microfibrillated Cellulose: Insights Gained from Experimental and Simulation Studies. *Ind. Eng. Chem. Res.* **2021**, *60*, 17663.
(29) Kadimi, A.; Benhamou, K.; Ounaies, Z.; Magnin, A.; Dufresne, A.; Kaddami, H.; Raihane, M. Electric Field Alignment of Nanofibrillated Cellulose (NFC) in Silicone Oil: Impact on Electrical Properties. *ACS Appl. Mater. Interfaces* **2014**, *6* (12), 9418−9425.
(30) Kalidindi, S.; Ounaies, Z.; Kaddami, H. Toward the Preparation of Nanocomposites with Oriented Fillers: Electric Field-Manipulation of Cellulose Whiskers in Silicone Oil. *Smart Mater. Struct.* **2010**, *19* (9), 094002.
(31) Wise, H. G.; Takana, H.; Ohuchi, F.; Dichiara, A. B. Field-Assisted Alignment of Cellulose Nanofibrils in a Continuous Flow-Focusing System. *ACS Appl. Mater. Interfaces* **2020**, *12* (25), 28568−28575.
(32) Bordel, D.; Putaux, J.-L.; Heux, L. Orientation of Native Cellulose in an Electric Field. *Langmuir* **2006**, *22* (11), 4899−4901.
(33) Kim, H. C.; Kim, J. W.; Zhai, L.; Kim, J. Strong and Tough Long Cellulose Fibers Made by Aligning Cellulose Nanofibers under Magnetic and Electric Fields. *Cellulose* **2019**, *26* (10), 5821−5829.
(34) Gindl, W.; Emsenhuber, G.; Maier, G.; Keckes, J. Cellulose in Never-Dried Gel Oriented by an AC Electric Field. *Biomacromolecules* **2009**, *10* (5), 1315−1318.
(35) Ten, E.; Jiang, L.; Wolcott, M. P. Preparation and Properties of Aligned Poly(3-Hydroxybutyrate-Co-3-Hydroxyvalerate)/Cellulose Nanowhiskers Composites. *Carbohydr. Polym.* **2013**, *92* (1), 206−213.
(36) Mahmoud, A.; Olivier, J.; Vaxelaire, J.; Hoadley, A. F. A. Electrical Field: A Historical Review of Its Application and Contributions in Wastewater Sludge Dewatering. *Water Res.* **2010**, *44* (8), 2381−2407.
(37) Probstein, R.F.6—Solutions of Electrolytes. In *Physicochemical Hydrodynamics*; Probstein, R. F., Ed.; Butterworth-Heinemann, 1989; pp 161−200. DOI: 10.1016/B978-0-409-90089-7.50012-1.
(38) Lockhart, N. C. Electroosmotic Dewatering of Clays. I. Influence of Voltage. *Colloids Surf.* **1983**, *6* (3), 229−238.
(39) Weber, K.; Stahl, W. Improvement of Filtration Kinetics by Pressure Electrofiltration. *Sep. Purif. Technol.* **2002**, *26* (1), 69−80.
(40) Brodin, F. W.; Theliander, H. Absorbent Materials Based on Kraft Pulp: Preparation and Material Characterization. *BioResources* **2012**, *7* (2), 1666−1683.
(41) Johansson, C.; Theliander, H. Measuring Concentration and Pressure Profiles in Deadend Filtration. *Filtration* **2003**, *3* (2), 114−120.
(42) Wetterling, J.; Mattsson, T.; Theliander, H. Local Filtration Properties of Microcrystalline Cellulose : Influence of an Electric Field. *Chem. Eng. Sci.* **2017**, *171*, 368−378.
(43) Basham, M.; Filik, J.; Wharmby, M. T.; Chang, P. C. Y.; El Kassaby, B.; Gerring, M.; Aishima, J.; Levik, K.; Pulford, B. C. A.; Sikharulidze, I.; Sneddon, D.; Webber, M.; Dhesi, S. S.; Maccherozzi, F.; Svensson, O.; Brockhauser, S.; Náray, G.; Ashton, A. W. Data Analysis WorkbeNch (DAWN). *J. Synchrotron Radiat* **2015**, *22* (3), 853−858.
(44) Lundahl, M. J.; Cunha, A. G.; Rojo, E.; Papageorgiou, A. C.; Rautkari, L.; Arboleda, J. C.; Rojas, O. J. Strength and Water Interactions of Cellulose I Filaments Wet-Spun from Cellulose Nanofibril Hydrogels. *Sci. Rep* **2016**, *6* (1), 30695.
(45) Ma, T.; Lv, L.; Ouyang, C.; Hu, X.; Liao, X.; Song, Y.; Hu, X. Rheological Behavior and Particle Alignment of Cellulose Nanocrystal and Its Composite Hydrogels during 3D Printing. *Carbohydr. Polym.* **2021**, *253*, 117217.
(46) Kafy, A.; Kim, H. C.; Zhai, L.; Kim, J. W.; Hai, L. V.; Kang, T. J.; Kim, J. Cellulose Long Fibers Fabricated from Cellulose Nanofibers and Its Strong and Tough Characteristics. *Sci. Rep* **2017**, *7* (1), 17683.
(47) Nissilä, T.; Wei, J.; Geng, S.; Teleman, A.; Oksman, K. Ice-Templated Cellulose Nanofiber Filaments as a Reinforcement Material in Epoxy Composites. *Nanomaterials* **2021**, *11* (2), 490.
(48) Baldrian, J. Effect of Swelling on the Structure of Oriented Polyamide 6. *Polymer* **1991**, *32* (4), 740−744.
(49) Lenz, J.; Schurz, J.; Wrentschur, E. The Fibrillar Structure of Cellulosic Man-Made Fibers Spun from Different Solvent Systems. *J. Appl. Polym. Sci.* **1988**, *35* (8), 1987−2000.
(50) Brännvall, E.; Larsson, P. T.; Stevanic, J. S. Changes in the Cellulose Fiber Wall Supramolecular Structure during the Initial

https://doi.org/10.1021/acs.iecr.2c03216
Ind. Eng. Chem. Res. XXXX, XXX, XXX−XXX

Stages of Chemical Treatments of Wood Evaluated by NMR and X-Ray Scattering. *Cellulose* **2021**, *28* (7), 3951−3965.
(51) Virtanen, T.; Penttilä, P. A.; Maloney, T. C.; Grönqvist, S.; Kamppuri, T.; Vehviläinen, M.; Serimaa, R.; Maunu, S. L. Impact of Mechanical and Enzymatic Pretreatments on Softwood Pulp Fiber Wall Structure Studied with NMR Spectroscopy and X-Ray Scattering. *Cellulose* **2015**, *22* (3), 1565−1576.
(52) Zhang, X.; Yu, Y.; Jiang, Z.; Wang, H. The Effect of Freezing Speed and Hydrogel Concentration on the Microstructure and Compressive Performance of Bamboo-Based Cellulose Aerogel. *J. Wood Sci.* **2015**, *61* (6), 595−601.
(53) Mittal, N.; Ansari, F.; Gowda V, K.; Brouzet, C.; Chen, P.; Larsson, P. T.; Roth, S. V.; Lundell, F.; Wågberg, L.; Kotov, N. A.; Söderberg, L. D. Multiscale Control of Nanocellulose Assembly: Transferring Remarkable Nanoscale Fibril Mechanics to Macroscale Fibers. *ACS Nano* **2018**, *12* (7), 6378−6388.
(54) Wetterling, J.; Jonsson, S.; Mattsson, T.; Theliander, H. The Influence of Ionic Strength on the Electroassisted Filtration of Microcrystalline Cellulose. *Ind. Eng. Chem. Res.* **2017**, *56* (44), 12789−12798.
(55) Chankuson, P.; Nisoa, M. Simulations of High Non-Uniform Electric Field in Dielectric Barrier Electrode System. *Walailak J.f Sci. Technol. (WJST)* **2021**, *18* (14), No. 12953.

https://doi.org/10.1021/acs.iecr.2c03216
Ind. Eng. Chem. Res. XXXX, XXX, XXX−XXX